Current Chemistry Letters 13 (2024) 367–376

Contents lists available at GrowingScience

Current Chemistry Letters

homepage: www.GrowingScience.com

Enhanced gas sensing performance of Ag-Doped $BiFeO_3$ microspheres synthesized via flash auto combustion technology

Amogh A. Sambare[a*] and Ramkisan Pawar[b]

[a]*Deen Dayal Upadhyay KAUSHAL Kendra, Dr Babasaheb Ambedkar Marathwada University, Aurangabad (MS), India*
[b]*Padmabhooshan Vasantdada Patil Institute of Technology, Savitribai Phule Pune University, Pune, India*

C H R O N I C L E

Article history:
Received March 20, 2023
Received in revised form
June 17, 2023
Accepted November 1, 2023
Available online
November 1, 2023

Keywords:
Gas sensing
Adsorption
Catalytic effect

A B S T R A C T

This investigation demonstrates the successful synthesis of well-crystallized pristine and Ag-doped $BiFeO_3$ microspheres using flash auto combustion technology. The effects of Ag doping on the morphology and microstructural characteristics were thoroughly examined through SEM, EDS, and powder X-ray diffraction (XRD) studies. Gas sensing experiments were performed to evaluate the response of the synthesized materials to NO gas. The results revealed a remarkable enhancement in the gas sensing capabilities of 5% wt Ag-doped $BiFeO_3$ compared to pure $BiFeO_3$. Specifically, the gas response towards NO was found to be 2.4 times higher for Ag-doped $BiFeO_3$. This significant improvement can be attributed to the presence of Ag atoms within the lattice structure, which not only increased the density of holes in the material but also created additional gas molecule adsorption sites. Furthermore, the Ag dopant exhibited a catalytic effect, contributing to the excellent gas sensor performance of the material. These findings hold great promise for the development of highly sensitive and efficient gas sensors, particularly in applications where the detection of low concentrations of NO is crucial. The utilization of flash auto combustion technology in the synthesis process offers a viable route for scalable production of advanced gas sensing materials with enhanced performance.

1. Introduction

One of the primary challenges faced by humanity today is environmental degradation caused by major hazardous pollutants, such as CO, NOx, and SOx. When these pollutants exceed their threshold limits, they have severe consequences for life on Earth [1]. Consequently, there is an increasing demand for simple, reliable, and affordable gas detection devices to measure and manage the quantity of these pollutants in the air [2]. Among the various gas detection materials, metal oxide-based gas detectors have gained attention from researchers due to their potential in addressing environmental concerns [3]. Binary metal oxides like ZnO, SnO_2, and Fe2O3 are often considered excellent semiconductor materials with high sensing capabilities [4,5]. However, their long-term reliability, especially in humid and warm environments, still remains a concern. Ternary metal oxides with perovskite ABO_3 structures have shown promise in providing more reliable and stable gas detection capabilities compared to binary metal oxides [6]. Bismuth ferrite oxide ($BiFeO_3$), one such perovskite material, is known for its multiferroic behavior, exhibiting both ferroelectric and antiferromagnetic properties at room temperature, making it a potential candidate for gas sensing applications, though research in this area is relatively limited [7-8].

Aliovalent dopants have been shown to improve the electrical and chemical sensitivities of oxide semiconductor sensors, enhancing their gas response and selectivity. Recently, multiferroic materials with a perovskite structure have garnered significant interest due to their potential applications in cutting-edge technology and environmentally friendly

* Corresponding author.
E-mail address asambare.ddukk@bamu.ac.in (A. A. Sambare)

doi: 10.5267/j.ccl.2023.10.008

materials [9]. Bismuth ferrite oxide ($BiFeO_3$) is an excellent example, with its ferroelectric and magnetic properties making it a promising candidate for use in radios, microwaves, storage devices, sensors, and intelligent devices[10]. Furthermore, several studies have highlighted the gas sensing capabilities of $BiFeO_3$ towards various common organic solvents, including alcohols, acetaldehyde, acetone, and ammonia, showcasing its potential in gas sensing applications [11-13]. To overcome the limitations of conventional binary metal oxide materials like SnO_2, ZnO, Co_3O_4, Fe_2O_3, etc., including long-term reliability, environmental effects, and high-temperature stability, there is an urgent need to investigate ternary metal oxide semiconductor gas detection materials. However, research in this area is currently insufficient.

In the existing literature, some studies have explored specific aspects of $BiFeO_3$ gas sensing properties and its response to certain gases. For instance, S. Neogi et al. [14] investigated the origin of the transition from irreversible to reversible acetone detection in Y-doped $BiFeO_3$ perovskites, which also demonstrated high output power and temperature sensing capabilities. Hongxiang Xue et al. [15] explored $BiFeO_3$ nanocrystals as a sensing material for isopropanol gas, showcasing exceptional gas-sensing properties. Toshi Bagwaiya et al. [16] studied the gas sensing properties of bismuth ferrite doped with silver, which exhibited an improved response and selectivity towards H_2S gas. G. Dong et al. [17] examined the impact of Ba substitution on the morphology, gas sensing, and electrical properties of bismuth ferrite. Qiang Li et al. [18] investigated the modification of bismuth ferrite nanospheres with Ag for enhanced chlorine gas sensing. Xue-Lian Yu et al. [19] discussed the gas-sensing properties of perovskite bismuth iron oxide nanoparticles synthesized through a soft chemical route, demonstrating ultralow sensing limits and excellent selectivity towards multiple organic gases. K. M. Zhu et al.[20] reported on the gas-sensing performance of walnut-shaped $BiFeO_3$ microspheres for detecting formaldehyde. S. Chakraborty et al.[21] developed a novel carbon monoxide gas sensor based on nanoparticles of bismuth ferrite, showcasing satisfactory response and stability. M. Dewan et al.[22] described the selective carbon monoxide sensing characteristics of the bismuth iron oxide (BFO) gas sensor, which exhibited high sensitivity and selectivity towards CO.

Table 1. Comparison of gas sensing characteristics of various pristine and doped bismuth ferrite nanostructures

Sensor Configuration	Test Gas	Optimum operating temperature (C)	Concentration (ppm)	Response (Rg/Ra)or (Rg-Ra/Ra)	Response Time (Sec)	Recovery Time (Sec)	Reference
Y- $BiFeO_3$	Acetone	350	50	17 (Rg-Ra/Ra)	25	---	14
$BiFeO_3$	Acetone	350	50	12 (Rg-Ra/Ra)	40	----	14
$BiFeO_3$	Isopropanol	240	100	31 (Rg/Ra)	6	17	15
Ba- $BiFeO_3$	Ethanol	400	100	14 (Rg/Ra)	3	10	17
$BiFeO_3$	Formaldehyde	240	200	3.0 (Rg-Ra/Ra)	20	14	20
$BiFeO_3$	CO	200	500	3.48 (Rg-Ra/Ra)	108	141	22
$BiFeO_3$	Ethanol	320	0.07 vol%	-----	30	80	23
$BiFeO_3$	Acetone	340	0.07 vol%	-----	40	80	25
La- $BiFeO_3$	Formaldehyde	100	50	23.3 (Rg/Ra)	5	30	27
$BiFeO_3$	SO_2	300	5	2.03 (Rg/Ra)	20	50	29
$BiFeO_3$	CO	350	30	2.12 (Rg/Ra)	25	13	31
$BiFeO_3$	NH_3	400	900	3 (Rg-Ra/Ra)	600	700	33
Tungsten doped $BiFeO_3$	NO_2	130	100	0.87 (Rg-Ra/Ra)	70	80	28
Tungsten doped $BiFeO_3$	H_2	130	100	0.78 (Rg-Ra/Ra)	95	100	28
Pd- $BiFeO_3$	NO_2	140	100	0.75 (Rg-Ra/Ra)	60	100	29
$BiFeO_3$	NO	200	10	2.4 (Rg-Ra/Ra)	130	285	This work
Ag- $BiFeO_3$	NO	200	10	7.5 (Rg-Ra/Ra)	120	456	This work

Overall, these studies provide valuable insights into the gas sensing capabilities of $BiFeO_3$ and its potential for environmental applications. However, further research is required to fully explore and understand the gas detection properties of ternary metal oxide semiconductor materials, especially considering the environmental challenges faced by the human race today.

It is indeed logical to explore the gas sensing capabilities of $BiFeO_3$, as this could open up new avenues for researching innovative multi-metal oxide semiconductor gas-sensitive materials simultaneously. Further investigation into the gas sensing properties of $BiFeO_3$ in combination with other metal oxides holds the potential to yield more reliable and stable gas sensing materials. Therefore, the primary focus of this work is on exploring the gas sensing capabilities of Ag-doped Bismuth Ferrite Oxides. The outcomes of this research could have significant implications for applications such as monitoring pollutants from automotive exhaust, ensuring workplace safety, and advancing healthcare systems, among other potential uses.

2. Materials and method

$Bi_{1-x}Ag_xFeO_3$; $0 < x < 0.2$ (BAFO) samples were synthesized using glycine as the fuel in an auto combustion reaction. The flash auto combustion method ensures uniform nanoparticle size distribution, high purity bismuth ferrite oxide, and rapid chemical reactions at high temperatures. Pure analar metal nitrates, such as iron nitrate $Fe(NO_3)_3 \cdot 9H_2O$, silver nitrate $Ag(NO_3)$, and $Bi(NO_3)_3 \cdot 5H_2O$, were combined in stoichiometric proportions to obtain the desired reactants. As per the findings of Ahmed et al., the quantity of glycine was calculated based on the total oxidizing and reducing coefficients of the

constituents to achieve a stoichiometric equilibrium, resulting in an equivalence ratio of one and maximum energy generation.

The reactants were heated on a magnetic stirrer and swirled, leading to thermal dehydration and the formation of a highly viscous gel. Upon further heating, the viscous gel expanded and ignited spontaneously, yielding a substantial amount of powder. The reaction occurred rapidly, producing a light, fluffy, and dry powder. This method is remarkably simple, fast, and cost-effective since it relies on an exothermic and self-sustaining chemical reaction between the metal salts and a suitable organic fuel, typically glycine or urea. The heat required for the chemical reaction is generated internally by the reaction itself, eliminating the need for an external heat source. The as-prepared nanopowders were subjected to X-ray diffraction analysis before being annealed in a muffle furnace at 600 °C for 2 hours.

2.1 XRD Characterization

The crystal structure and grain size of both pure and silver-doped $BiFeO_3$ powders, annealed at 600 degrees Celsius, were assessed using X-ray diffraction. Figure 1(a) depicts the XRD spectra of pure $BiFeO_3$ and $BiFeO_3$ doped with 5% wt, 10% wt, 15% wt, and 20% wt of silver. The main peaks were observed at $2\theta = 22.5$ and 32.08, corresponding to the Miller indices (104) and (110), respectively, in the rhombic $BiFeO_3$ crystal structure (JCPDS #01-073-0548). The XRD results indicate that both pure and doped $BiFeO_3$ powders are crystalline in nature after annealing at 600 degrees Celsius.

Using a Cu-K radiation source, X-ray powder diffraction patterns (XRD) were generated and analyzed using a Bruker model. The analysis revealed that the dominant phase is crystallized in a rhombohedral-hexagonal lattice, and the prepared samples exhibit a high degree of crystallinity, as indicated by the intensity of the peaks [21].

The pure Ag-doped $BiFeO_3$ thick film sensor, with varying dopant concentrations of 5% wt, 10% wt, 15% wt, and 20% wt, showed average particle sizes of 30 nm, 32 nm, 30 nm, and 33 nm, respectively. The presence of Ag dopant atoms led to a reduction in the crystallite size of the BFO structure. This reduction in size can cause broadening of the (110) peak in the XRD pattern, resulting in a smooth valley in the intensity profile of the peak. Thus, XRD analysis revealed that the annealed samples have a nanocrystalline structure.

The XRD spectra were used to investigate the phase arrangement, crystallinity, and purity of the obtained BFO and Ag-BFO powders. The wide, low-intensity XRD lines suggested that the particles possess a nanoscale structure. When compared to pure BFO, the intensity of the (012) peak decreased by 78% in the case of 5% wt Ag-doped BFO, 60% in the case of 10% wt Ag-doped BFO, 60% in the case of 15% wt Ag-doped BFO, and 10% in the case of 20% wt Ag-doped BFO. Similar trends were observed for the (104) peak, and this phenomenon could be attributed to the signal attenuation caused by Ag molecules. However, beyond 15% wt Ag doping, the peaks of BFO were not affected.

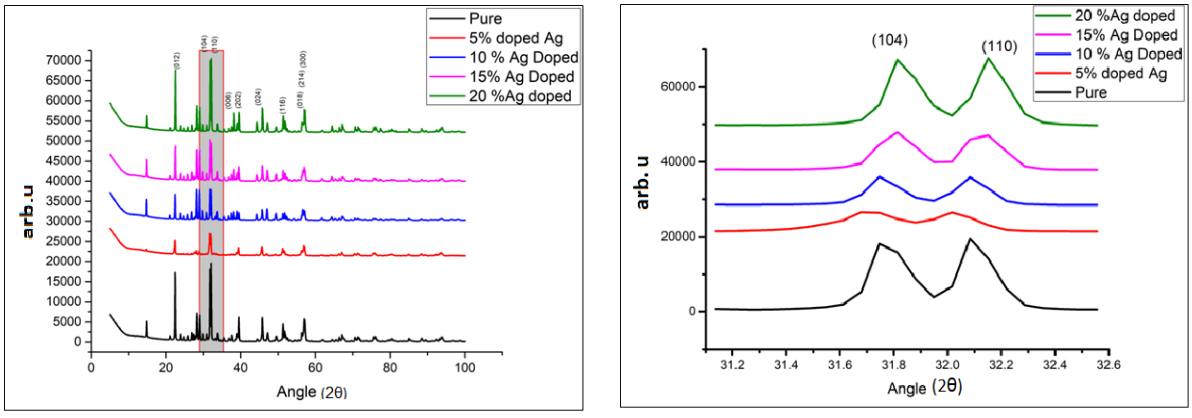

(a) (b)

Fig. 1: (a) XRD plot of BFO and Ag-BFO (Angle 2θ Vs arb.u) (b) Magnified XRD plot of BFO and Ag-BFO Angle (2θ)

2.2 Scanning Electron Microscopy

Fig. 2 present the SEM micrographs of the pure and silver-doped $BiFeO_3$ thick film sensors. The process of calcination removes organic components from the nano powders, leading to diffusion, accumulation, and elevated crystallization of the $BiFeO_3$ nano powders near the surface, resulting in the formation of internal porous $BiFeO_3$ microcubes[24]. The microstructure and surface are two key factors that significantly influence sensor properties. The presence of high concentrations of atoms at the pore surfaces and interfaces indicates that the microstructure of the porous membrane is well-suited for gas detection. In other words, the ample exposure of adsorbed surface sites to the chemical environment contributes to the high sensitivity of the sensor. The SEM images vividly illustrate the highly porous surfaces of our thick film sensors, making them highly suitable for sensing applications. The SEM images reveal slight variations in grain size compared to the grain sizes predicted by XRD measurements, as XRD is used to establish the average particle size. This

change in size is likely due to grain aggregation, as evidenced in the SEM image. Another observation is that samples with x = 5% exhibit more favorable grain growth direction. The particles in the photos appear nearly spherical and clustered, and this aggregation could be a result of the magnetic properties of the BFO nanoparticles.

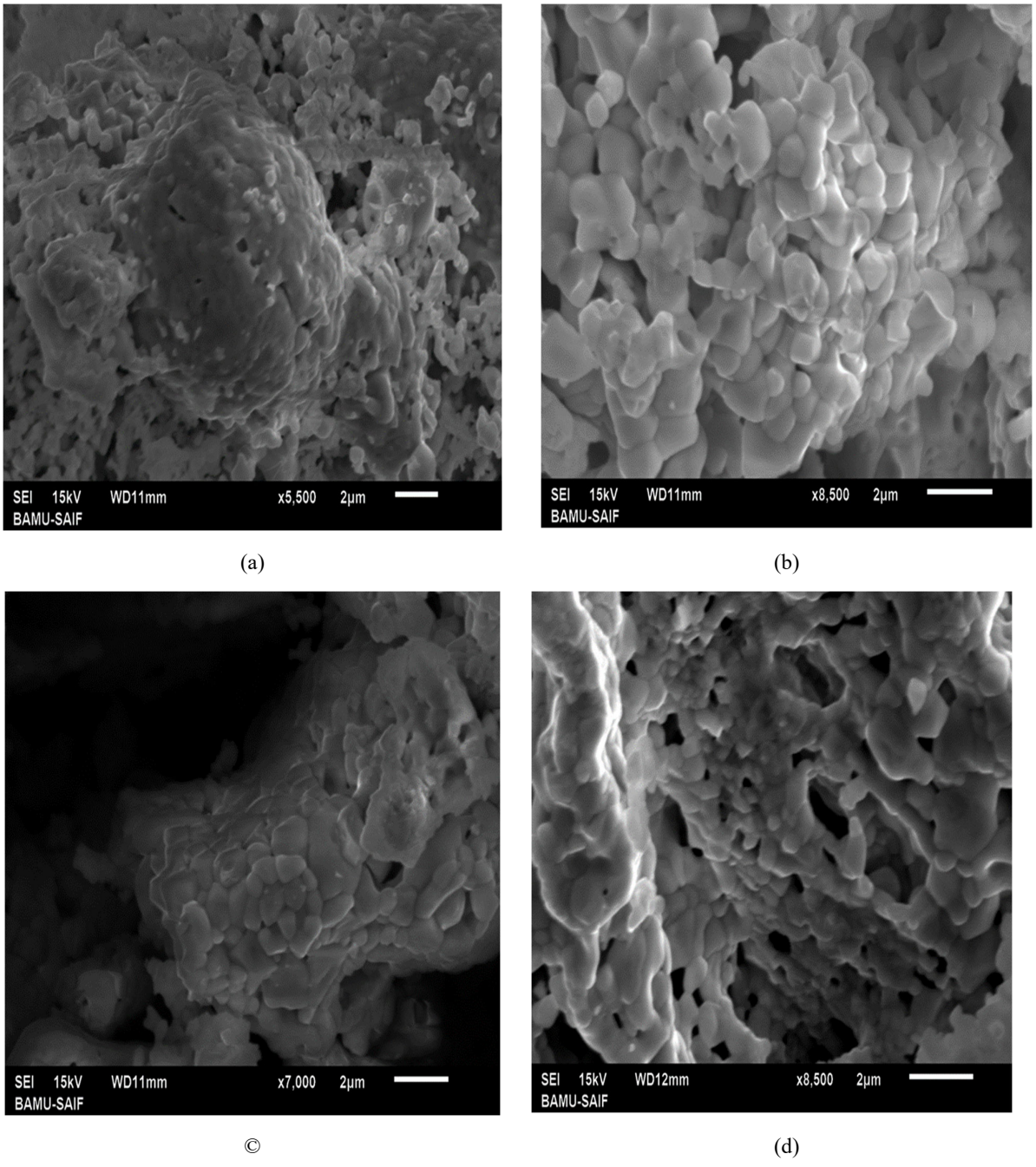

Fig. 2: (a) SEM Image for Bismuth Ferrite Oxide ($BiFeO_3$) (b) SEM Image for 5 % wt Ag Doped $BiFeO_3$ (c) SEM Image for 10 % wt Ag Doped $BiFeO_3$ (d) SEM Image for 15 % wt Ag Doped $BiFeO_3$

2.3 EDS

Fig. 3 (a) display the EDS spectra of a pure $BiFeO_3$ thick film sensor annealed at 600°C. Fig. 7 reveals the presence of only bismuth, iron, and oxygen in its spectrum. Fig. 3 (b), on the other hand, shows the EDS spectrum of the 1.5% wt silver-doped $BiFeO_3$ thick film sensor. The spectroscopy analysis confirms the presence of silver in the doped samples.

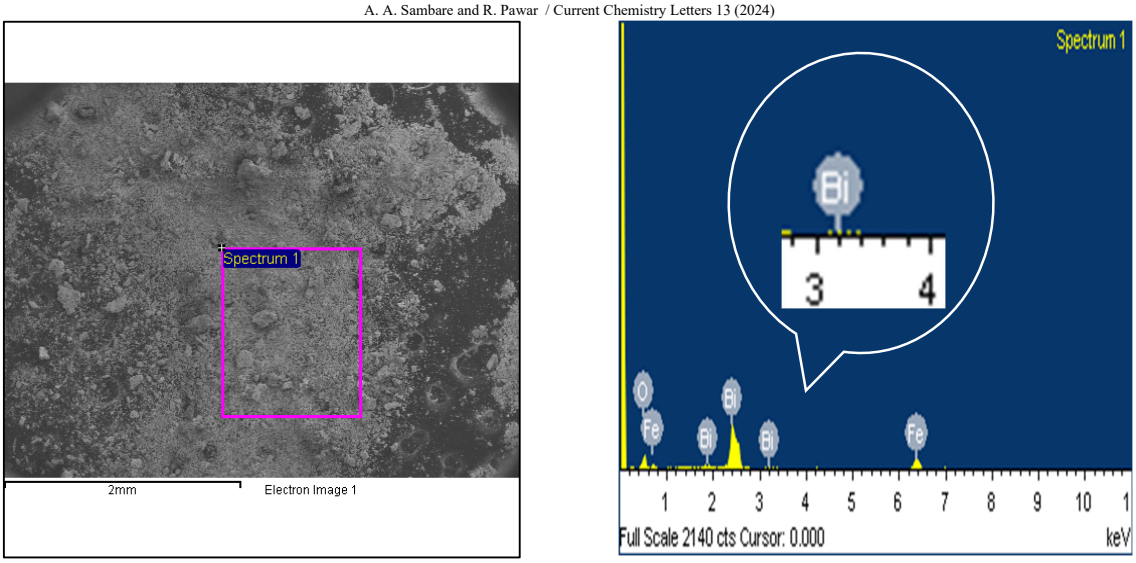

(a)

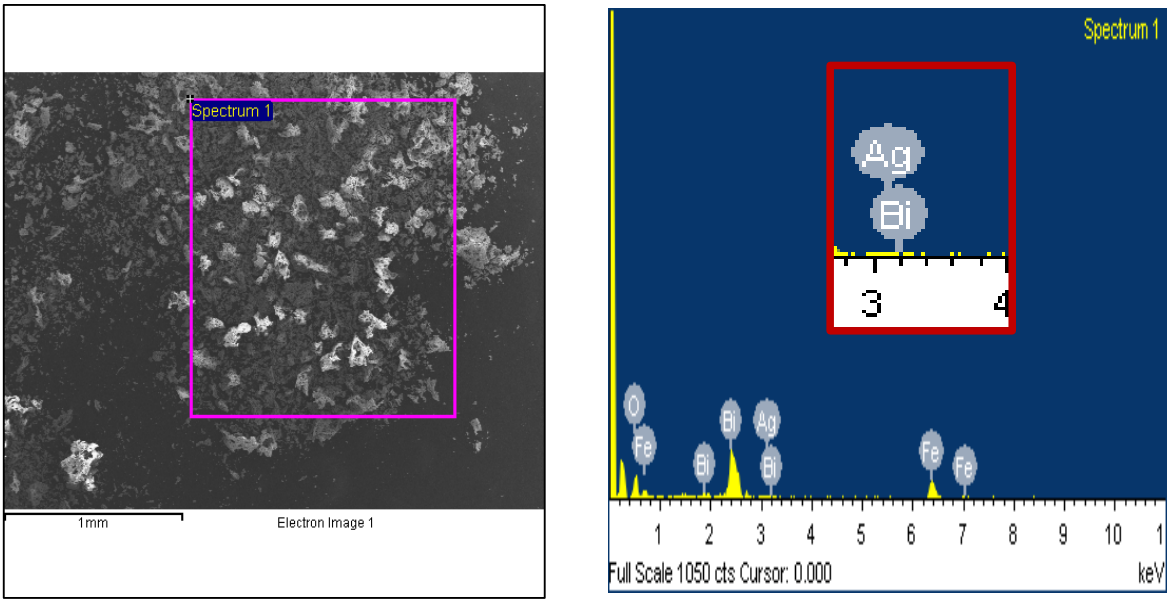

(b)

Fig. 3. (a) EDS for $BiFeO_3$ (b) EDS for Ag-$BiFeO_3$

2.4 FTIR

The FTIR (Fourier Transform Infrared) spectroscopy technique was utilized to investigate the vibrational modes of molecules and materials, providing valuable information about the chemical bonding and structural properties of BFO and Ag-doped BFO.

In the case of BFO, strong infrared absorption bands are observed in the range of approximately 400-600 cm^{-1}, which can be attributed to the stretching and bending vibrations of the Fe-O and Bi-O bonds in the crystal lattice. When Ag is doped into the BFO material, additional absorption bands may appear in the FTIR spectra due to the presence of Ag-O bonds. These bands are usually observed at higher frequencies than the Fe-O and Bi-O bonds in BFO, typically around 700-800 cm^{-1}. The appearance of these Ag-O bands is indicative of the successful incorporation of Ag dopants into the BFO lattice.

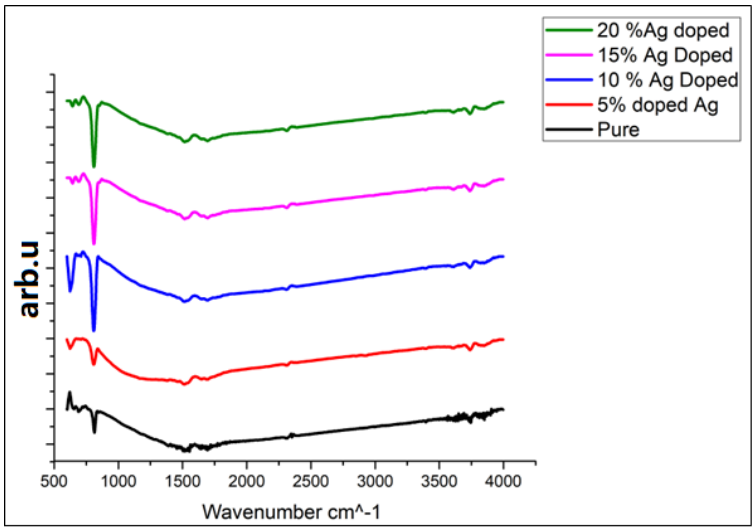

Fig. 4. FTIR Plot for BFO and Ag-BFO

2.5 Gas Sensing Set-up

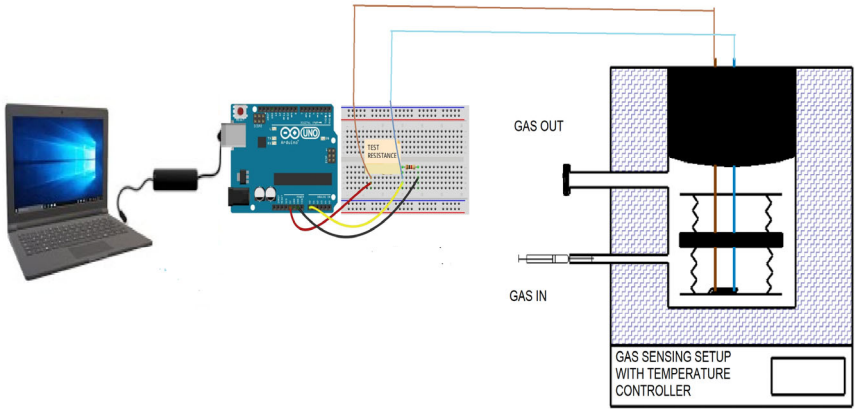

Fig. 5. Static gas sensing setup for gas sensing measurement.

In this section, we describe the gas sensing set-up that was utilized to assess the gas sensing abilities of the synthesized $BiFeO_3$ and Ag-doped $BiFeO_3$ materials.

The gas sensing experiments were conducted using a custom-designed static gas sensing set-up. Static sensors are ideal for maintaining a constant sample and temperature, leading to more stable and consistent gas detection. The gas sensor unit comprised a stainless steel (SS) cylinder-shaped compartment with a volume size of 250 mL. This cylinder-shaped compartment was connected to a heater with a PID controller to maintain the desired temperatures during the experiments.

To measure the change in resistance of the gas sensor due to the presence of the target gas, we employed an Arduino Uno Ohmmeter system. The Arduino Uno Ohmmeter was connected to the computer via a USB interface to record the changes in resistance over time.

For the fabrication of the gas sensors, 200 mg of the obtained sample powder nanocrystals were mixed with 0.2 mL of HCl by grinding in an agate mortar to form a paste. This paste was thinly deposited on the surface of a fluorine-doped tin oxide (FTO) coated glass substrate. The FTO glass substrate has a resistivity of less than 15 ohms per square meter. Subsequently, the paste on the FTO glass was dried to create planar gas sensors for gas sensing purposes. Before the actual gas sensing experiments, the dried sensors were aged at 200°C for 10 hours in air.

To study the temperature dependence of the sensor's response to NO gas molecules, the 0.05 wt% Ag-doped BFO film sensor was tested at varying temperatures ranging from 100 to 350 °C (as shown in Fig. 6). The sensor response was quantified using Response versus Time in Seconds, where Response = $(R_{gas} - R_{air}) / R_{air}$. Here, R_{gas} represents the resistance of the sensor in the presence of the gas, and R_{air} is the resistance of the sensor before gas exposure.

Our study focused on the NO gas sensing ability of both pristine BFO and 0.05% wt Ag-BFO within the temperature range of 100 to 350 °C. The sensor's sensitivity was found to increase up to around 200 °C and then started to decline. Fig. 6 illustrates the response and recovery characteristic curves of the 0.05 wt% Ag-doped BFO film sensor for NO gas sensing at various temperatures.

The optimal operating temperature, offering the best balance between sensor responsiveness and dynamics, was found to be 200 °C. At this temperature, the sensor achieved the highest response with a response time of 120 seconds and a recovery time of 7.6 minutes. Further studies were conducted at this temperature to analyze the sensor's response to various NO gas concentrations, ranging from 5 ppm to 40 ppm. The obtained readings showed a minimum response of 2.1 and a maximum of 18.1 (as depicted in Fig. 7).

Overall, the gas sensing set-up provided a reliable platform for assessing the gas sensing performance of both pristine BFO and Ag-doped BFO materials, revealing valuable insights into their gas sensing capabilities.

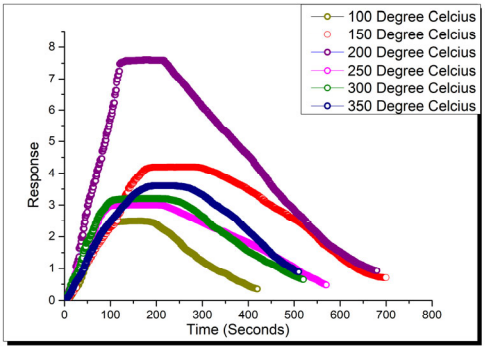

Fig. 6. NO gas sensing on 5% wt Ag-BFO in temperature range of 100-350 °C.

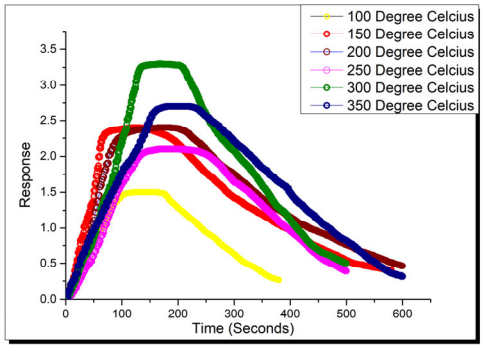

Fig. 7. NO gas sensing on-BFO in temperature range of 100-350 °C.

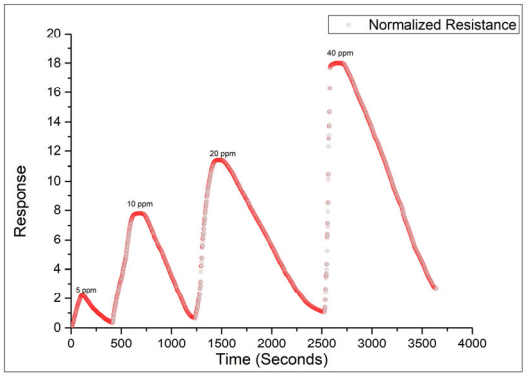

Fig. 8. 5-40 ppm NO gas sensing on 5 % wt Ag-BFO at 200 °C.

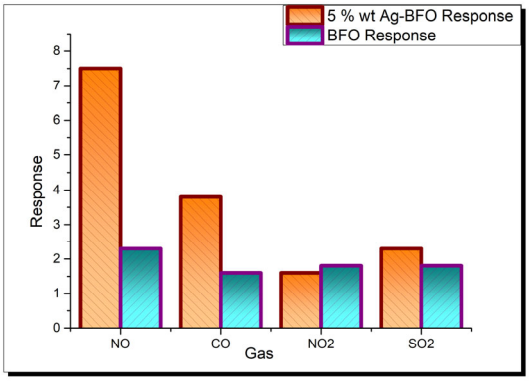

Fig. 9. Response of various gas species to BFO and Ag-BFO at 200 °C.

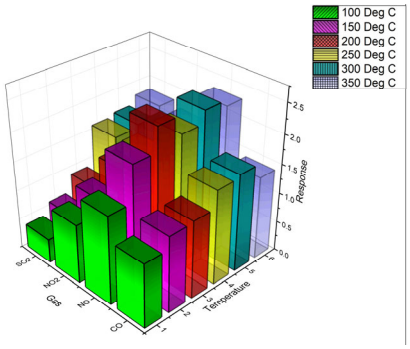

Fig. 10. Cross selectivity of various gases towards BFO at different temperatures.

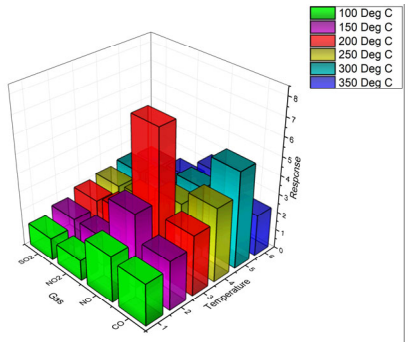

Fig. 11. Cross Selectivity of various gases towards 5 wt % Ag-BFO at different temperatures.

4. Results and Discussion

The electrical properties of a typical semiconductor, such as $BiFeO_3$, show a decrease in resistance with increasing temperature in air. $BiFeO_3$ is a non-stoichiometric oxide known to possess oxygen vacancies both on its surface and inside its structure. The amount of oxygen ions adsorbed on $BiFeO_3$ nanocrystals varies with temperature, affecting the interaction with NO gas molecules. To determine the optimal operating temperature for NO detection, the gas response (measured by sensitivity) of the $BiFeO_3$ gas sensor to 10 ppm NO gas at temperatures ranging from 100°C to 350°C was investigated (Fig. 6).

For the Ag-doped BFO sensor, the NO sensitivity initially increases with rising temperature, peaking at 200°C, and then gradually decreases. Similarly, when pure $BiFeO_3$ is used for NO gas detection, the response gradually increases with temperature and achieves the best reaction at 300°C. However, as the temperature continues to rise beyond this point, the response to NO gas decreases. This is because NO gas molecules require a specific amount of thermal energy to react with surface-adsorbed oxygen species. At very high temperatures, the desorption rate of oxygen gas increases, causing a considerable number of adsorbed oxygen atoms to leave before reacting with NO gas molecules. Consequently, the response to NO gas decreases.

The ideal operating temperature is the one at which the adsorption and desorption processes are in equilibrium. For the $BiFeO_3$ nanocrystalline Ag-doped NO sensor, the highest response value is observed at 200°C, which is considered the optimum operating temperature.

The holes in the BFO nanospheres migrate to Ag when Ag is doped into the BFO structure, which lowers the positive charge on the BFO nanospheres and causes the conduction and valence bands to bend downward. Ag and BFO nanospheres are separated by an energy potential barrier as a result. As a result of the electron-hole separation, there are fewer electrons in the conduction band, which increases the likelihood that electrons will connect with surface O_2 and NO and speed up the process.

Additionally, Ag particles serve as unique O_2 and NO adsorption sites, and the interface between Ag and BFO may develop a Schottky junction. As a result, the interfacial effect is enhanced, and the grain boundary barrier is lowered. A faster saturation of the reaction is made possible by the fact that carriers migrate quickly from BFO to Ag, leaving more electrons accessible at the reaction sites. As a result, both the gas reaction and the response time are greatly enhanced [31-32].

5. Conclusion

For the purpose of detecting NO gas, we have successfully created a gas sensor employing Ag-doped $BiFeO_3$ (Ag-BFO). We carefully examined the phase composition, surface appearance, and chemical characteristics of Ag-doped $BiFeO_3$ nanospheres by extensive research. We also carefully looked into the sensor's ability to detect gases. The outcomes shown that Ag-BFO displayed higher sensitivity to NO gas compared to pure $BiFeO_3$, exhibiting a spectacular NO gas response of 7.5 to 10 ppm at an ideal operating temperature of 200°C. Additionally, in its prepared state, the Ag-BFO sensor showed remarkable selectivity.

Also, the addition of Ag dopants, which considerably improved the performance of the sensor as a whole. They raised the hole density and the quantity of gas adsorption sites while also having a catalytic impact. Overall, the addition of Ag metal doping to the perovskite $BiFeO_3$ structure creates new opportunities for enhancing the gas sensitivity and selectivity of gas sensors. Advanced gas detection technologies are being developed as a result of this study, and they might be used in a number of industries, including healthcare, workplace safety, and environmental monitoring. Future solutions to environmental issues and advancements in gas detection systems might be achieved using the Ag-doped $BiFeO_3$ sensor.

References

1. E. Fauré, Å. Svenfelt, G. Finnveden, and A. Hornborg, **(2016)** "Four sustainability goals in a Swedish low-growth/degrowth context," *Sustain.*, 8 (11) 1–18.
2. S. Tajik *et al.*, **(2021),** "Recent developments in polymer nanocomposite-based electrochemical sensors for detecting environmental pollutants," *Ind. Eng. Chem. Res.*,60 (3) 1112–1136.
3. M. M. McCartney *et al.*, **(2017)**, "An Easy to Manufacture Micro Gas Preconcentrator for Chemical Sensing Applications," *ACS Sensors.*, 2 (8) 1167–1174.
4. Mikami, K., Kido, Y., Akaishi, Y., Quitain, A., & Kida, T. **(2019)**. Synthesis of Cu2O/CuO Nanocrystals and Their Application to H2S Sensing. *Sensors*, *19*(1), 211.
5. P. S. Kolhe, P. M. Koinkar, N. Maiti, and K. M. Sonawane, **(2017),** "Synthesis of Ag doped SnO_2 thin films for the evaluation of H2S gas sensing properties," *Phys. B Condens. Matter*, 524 (7) 90–96.
6. A. Bala, S. B. Majumder, M. Dewan, and A. Roy Chaudhuri, **(2019)**, "Hydrogen sensing characteristics of perovskite based calcium doped $BiFeO_3$ thin films," *Int. J. Hydrogen Energy*, 44 (33) 18648–18656.
7. D. Rathore, R. Kurchania, and R. K. Pandey, **(2015)**, "Gas Sensing Properties of Size Varying CoFe2O4 Nanoparticles," *IEEE Sens. J.*, 15 (9) 4961–4966.

8. Dziubaniuk, M., Bujakiewicz-Korońska, R., Suchanicz, J., Wyrwa, J., & Rękas, M. **(2013)**. Application of bismuth ferrite protonic conductor for ammonia gas detection. Sensors and Actuators B: Chemical, 188, 957–964.
9. Rao, S. K., Kalai Priya, A., Manjunath Kamath, S., Karthick, P., Renganathan, B., Anuraj, S., . . . Gopalakrishnan, C. **(2020)**. Unequivocal evidence of enhanced room temperature sensing properties of clad modified Nd doped mullite Bi2Fe4O9 in fiber optic gas sensor. Journal of Alloys and Compounds, 838, 155603..
10. J. S. Hwang *et al.*, "Reinforced magnetic properties of Ni-doped $BiFeO_3$ ceramic," **(2016)** *J. Korean Phys. Soc.*, 69 (3) 282–285.
11. P. Kumar and P. Chand, **(2018)**, "Structural, electric transport response and electro -strain - Polarization effect in La and Ni modified bismuth ferrite nanostructures," *J. Alloys Compd.*, 748 504–514.
12. J. Łojewska, A. Knapik, P. Jodłowski, T. Łojewski, A. Kołodziej, **(2013)** Topography and morphology of multicomponent catalytic materials based on Co, Ce and Pd oxides deposited on metallic structured carriers studied by AFM/Raman interlaced microscopes, *Catal. Today*, 216 11–17.
13. P.J. Jodłowski, D. Chlebda, E. Piwowarczyk, M. Chrzan, R.J. Jędrzejczyk, M. Sitarz, A. Węgrzynowicz, A. Kołodziej, J. Łojewska, **(2016)** In situ and operando spectroscopic studies of sonically aided catalysts for biogas exhaust abatement, *J. Mol. Struct.* 1126, 132–140.
14. S. Neogi and R. Ghosh, **(2020)**, "Origin of irreversible to reversible transition in acetone detection for Y-doped $BiFeO_3$perovskite," *J. Appl. Phys.*, 128 (14).
15. H. Xu, J. Xu, J. Wei, and Y. Zhang, **(2020)**, "Fast response isopropanol sensing properties with sintered $BiFeO_3$ nanocrystals," *Materials (Basel).*, 13 (17).
16. T. Bagwaiya *et al.*, **(2018)**, "Investigation on gas sensing properties of Ag doped $BiFeO_3$," *AIP Conf. Proc.*,1942 1–5.
17. G. Dong, H. Fan, H. Tian, J. Fang, and Q. Li, **(2015)**, "Gas-sensing and electrical properties of perovskite structure p-type barium-substituted bismuth ferrite," *RSC Adv.*,5 (38) 29618–29623.
18. Q. Li, W. Zhang, C. Wang, J. Ma, L. Ning, and H. Fan, **(2018)**, "Ag modified bismuth ferrite nanospheres as a chlorine gas sensor," *RSC Adv.*, 8 (58) 33156–33163.
19. X. L. Yu, Y. Wang, Y. M. Hu, C. B. Cao, and H. L. W. Chan, **(2009)**, "Gas-sensing properties of perovskite $BiFeO_3$ nanoparticles," *J. Am. Ceram. Soc.*, 92, (12) 3105–3107.
20. K. M. Zhu *et al.*, **(2019)**, "Preparation, characterizaton and formaldehyde gas sensing properties of walnut-shaped BiFeO 3 microspheres," *Mater. Lett.*, 246, 107–110.
21. S. Chakraborty and M. Pal, **(2018)**, "Highly efficient novel carbon monoxide gas sensor based on bismuth ferrite nanoparticles for environmental monitoring," *New J. Chem.*, 42 (9), 7188–7196.
22. M. Dewan and S. B. Majumder, **(2019)**, "Selective carbon monoxide sensing properties of bismuth iron oxide," *Materialia*, 7 (2).
23. G. M. Albino, O. Perales-Pérez, B. Renteria-Beleño, and Y. Cedeño-Mattei, **(2014)**, "Effect of Ca and Ag doping on the functional properties of BiFeO 3 nanocrystalline powders and films," *MRS Proc.*,1675 105–111.
24. Q. Yu, Y. Zhang, and Y. Xu, **(2021)**, "Hierarchical hollow $BiFeO_3$microcubes with enhanced acetone gas sensing performance," *Dalt. Trans.*, 50 (19) 6702–6709.
25. Kuo-Chin Hsu, Te-Hua Fang, Shinn-Horng Chen, En-Yu Kuo, **(2019)**,Gas sensitivity and sensing mechanism studies on ZnO/La0.8Sr0.2Co0.5Ni0.5O3 heterojunction structure, Ceramics International, 45 (7) 8744-8749, ISSN 0272-8842.
26. C.A. Neto , J.I. Yanagihara , F. Turri , **(2008)**, A carbon monoxide transport model of the hu- man respiratory system applied to urban atmosphere exposure analysis, *J. Braz. Soc. Mech. Sci. Eng*., 30 253–260 .
27. G.F. Fine , L.M. Cavanagh , A. Afonja , R. Binions , **(2010)** Metaloxide semi-conductor gas sen- sors in environmental monitoring, *Sensors* .,10 5469–5502.
28. S. D. Waghmare, V. V. Jadhav, S. F. Shaikh, R. S. Mane, J. H. Rhee, and C. O'Dwyer, **(2010)**, "Sprayed tungsten-doped and undoped bismuth ferrite nanostructured films for reducing and oxidizing gas sensor applications," *Sensors Actuators, A Phys*., 271, 37–43.
29. S. D. Waghmare et al., **(2020)**, "Pristine and palladium-doped perovskite bismuth ferrites and their nitrogen dioxide gas sensor studies," J. King Saud Univ. – 32 (7) 3125–3130.
30. M. A. Ahmed, S. F. Mansour, S. I. El-Dek, and M. Abu-Abdeen, **(2014)**, "Conduction and magnetization improvement of $BiFeO_3$ multiferroic nanoparticles by Ag+ doping," *Mater. Res. Bull*., 49 (1) 352–359.
31. Sambare, A.A., Datta, K.P., Shirsat, M.D., R.S.Pawar, **(2022)** Adsorption of gas molecules (CO, CO2, NO, NO2, and CH4) on undoped and Ag-doped bismuth ferrite oxide (BFO) by DFT investigation, *Journal of Materials Research*., 37, 4296–431.
32. Sambare, A.A., Pawar, R. & Shirsat, M., **(2023)**, A DFT investigation on transition metal (Co, Cr, Cu, Mn, Mo and Nb)-doped bismuth ferrite oxide (BiFeO3) for CO gas adsorption,*Theor Chem Acc*.,142, 61.